Experiments in Fluids (2023) 64:90
https://doi.org/10.1007/s00348-023-03625-8

RESEARCH ARTICLE

Focused, high-speed liquid jets induced via low-voltage sparks in capillary tubes

Pankaj Rohilla[1,2] · **Jeremy Marston**[1]

Received: 2 September 2022 / Revised: 11 January 2023 / Accepted: 23 March 2023 / Published online: 24 April 2023

Abstract

When a high-voltage capacitor is discharged between two electrodes in a conducting liquid, the resulting spark can create a rapidly expanding cavitation bubble. We exploit this phenomenon in capillary tubes to create high-speed liquid jets that could be used for several applications, including drug delivery, surface coating, inkjet printing, etc. We conducted a systematic study to understand the role of various parameters, such as fluid viscosity, location of the spark point, and discharge voltage, on the jet dynamics and show that all three parameters of the system have a statistically significant effect. Overall, we observed focused jets with diameters $\mathcal{O}(10^{-4} - 10^{-3})$ m, and speeds in the range $\mathcal{O}(10^{1}$–$10^{2})$ m/s, yielding typical jet Reynolds numbers $Re_j \sim \mathcal{O}(10^3 - 10^4)$. For viscous fluids and low voltages, we were able to produce discrete droplets. However, in the jet regime, the speed can be tuned by the discharge voltage and the location of the spark point relative to the center of the meniscus. In addition to basic jet hydrodynamics, we also report experiments in which this jetting mechanism is used to deposit liquid onto substrates placed below the open end of the capillary. We propose that this system can generate focused liquid jets useful for coating with viscous liquids, and potentially for needle-free jet injections.

1 Introduction

Cavitation bubbles have been studied widely to understand the magnitude of damage they can cause on moving parts of turbomachinery dealing with fluid flow such as pumps and impellers (e.g., Brennen 2014; Osman et al. 2022). In particular, it is the violent collapse of these cavitation bubbles (a.k.a. "Rayleigh implosion mechanism", Blake and Gibson (1987)) which is most destructive, when the close proximity of a solid surface leads to the generation of high-speed liquid jets focused toward that surface. This process and the associated water hammer effect have been well documented both experimentally and numerically. Due to the strong influence of the bubble-boundary interaction, a lot of research has also been done to understand the role of material stiffness in cavitation erosion (Blake and Gibson 1987; Chaves et al. 1995; Brujan et al. 2001).

Historical evidence for experiments using sparks to create bubbles dates back to World War II, where spark-induced cavitation was used to simulate damage to ships caused by underwater explosions (Burrill 1951; Davies and Taylor 1943). Spark-induced cavitation has since been widely studied to understand the effects of wall proximity, free surfaces, particles, and other bubbles near the cavitation bubble (Blake and Gibson 1987; Kling and Hammitt 1970; Shima et al. 1983; Vandiver and Wales 1977). Several techniques have been used to generate cavitation bubbles such as laser focusing, impact-driven shock-waves, etc. (Dijkink and Ohl 2008; Tagawa et al. 2012; Gordillo et al. 2020); however, spark-induced cavitation based on low-voltage discharge is an inexpensive and simple technique to yield consistent bubbles (Goh et al. 2013; Podbevsek et al. 2021).

In a similar fashion to focused laser pulses in liquids contained in restricted geometries (Tagawa et al. 2012, 2013; Rohilla and Marston 2020), spark-induced cavitation within a liquid can also be harnessed to generate high-speed liquid microjets (Karri et al. 2012; Avila et al. 2015). These microjets have several applications such as precise low-volume drug delivery, inkjet printing, and surface coating (Fletcher et al. 2002). Although prior research has studied spark-induced jetting from open air-water interfaces, a systematic

✉ Jeremy Marston
jeremy.marston@ttu.edu

[1] Department of Chemical Engineering, Texas Tech University, Lubbock, TX, USA

[2] Present Address: Georgia Institute of Technology, Atlanta, GA, USA

study of the generation of focused jets from capillary tubes using spark-induced cavitation has not yet been performed.

In this study, we characterize the dynamics of spark-induced jets from capillary tubes and conduct a parametric study to highlight the role of various parameters on the shape and speed of these liquid jets. We use a low-voltage (25–60 V) discharge technique to generate focused jets by discharging at a desired point inside a transparent tube containing liquid. We used brass wires as electrodes to avoid the wire break-off after a spark which has been observed in earlier studies using copper wires (Lew et al. 2007). Specifically, we investigate the effect of capacitance, voltage, fluid viscosity, and length between the meniscus and the spark point on the shape and the speed of the jet. In addition, we provide an illustrative example of deposition onto a substrate placed below the open end of the capillary.

2 Materials and methods

2.1 Spark generation device

Figure 1 shows the device used to create spark-induced jets. This device houses a basic RC circuit (Fig. 1A), where a capacitor was charged through a 1 kΩ resistor and discharged when needed using a toggle switch (*Nilight 90012E Heavy Duty Rocker, 15A (250V)/20A (125V) SPST 2 Pin*). We used two capacitors (*1000 μ F and 4700μF, 63 V, Aluminum Electrolytic Capacitor, Nichicon*) in this study. All electrical components were then transferred to a printed circuit board (*Oshpark board printing services*) shown in Fig. 1(B,C). The body of the spark-jet device (Fig. 1D) was printed using a 3D printer (*Formlabs Inc.*) with a gray resin. Figure 1(E) shows an assembled spark-jet device.

A 12 V DC power supply was used in conjunction with a voltage booster (*Oumefar Boost 1500 W 30A DC-DC Converter Step-up*) to generate voltages in the range of 25–60 V.

2.2 Materials

Brass wires (1/32", *K & S Precision Metals*) were used as electrodes to discharge the voltage at a point inside a liquid stored in a transparent polycarbonate tube (D_i = 3.2 mm, D_o = 6.3 mm, *Plasticraft*) or in a glass tank (for visualization purposes only). As indicated in Fig. 1F, the distance between the spark point and the meniscus, L_m, was variable and, for purposes of this study, ranged between 3 and 11 mm. DI water, 50%$_{w/w}$ glycerol (*Macron Fine Chemicals*) and 80%$_{w/w}$ glycerol were used to generate liquid jets. The physical properties of these fluids are presented in Table 1.

Table 1 Physical properties of the fluids used. Thermal conductivities are based on values in [22], and dielectric constants are based on values in Albright (1937)

	DI Water	50% glycerol	80% glycerol
ρ (kg/m^3)	~996	~1130	~1209
μ (mPa s)	~1	~6.9	~84
k (W/m·K)	0.609	0.415	0.327
κ	80.37	65.63	52.57

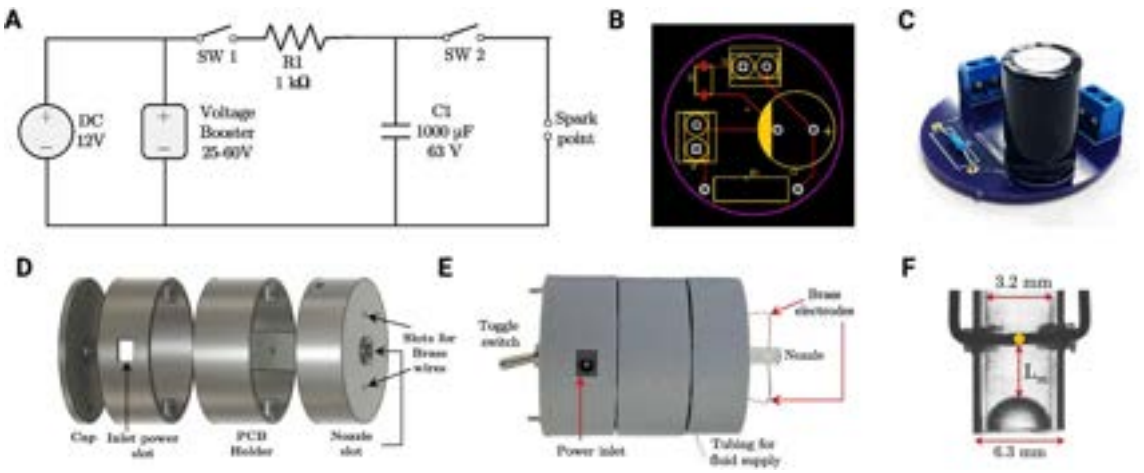

Fig. 1 Experimental setup. **A** Circuit diagram of the spark-induced jetting device, **B** PCB with the same circuit, **C** PCB with mounted electrical components, **D** expanded view of the jet generation device, **E** assembled view of the spark device used to generate drops and high-speed jets, **F** polycarbonate tube annotated with dimensions, showing the location of the spark point (yellow circle), meniscus, and the definition of L_m (≈ 3 mm in this figure)

2.3 Imaging

Direct imaging of the cavitation bubble inside the capillary tubes presented difficulties due to small scale and curvature of the tubing, so to provide initial observations of the cavitation bubble expansion and collapse, a limited number of trials were performed in a glass tank, captured at 40,000 fps using a Photron high-speed camera (*Fastcam Nova S6, Photron Inc.*) with a resolution of 512×384 and an exposure time of 900 μs.

To record the dynamics of liquid jets from capillary tubes, we used a Phantom high-speed camera (*Phantom v711, Vision Research Inc.*) at a frame rate of 20,000 fps for a resolution of 208×800 and an exposure time of 30 μs. To prevent saturation of the camera sensor from intense photoemissions from the spark, we used two neutral density filters (ND×4, Hoya). The effective pixel size ranged from 20-100 μm depending on the magnification used. Photron FASTCAM Viewer (PFV4) and ImageJ were both used to perform various image analyses including measurement of jet diameters and cavitation bubbles sizes. Of particular interest was the jet speed, where we tracked the jet tip frame by frame from the first formation that emerges from the meniscus.

2.4 Statistical analysis

One-way ANOVA tests with significance levels of $\alpha = 0.01$ (*high significance*) and $\alpha = 0.05$ (*low significance*) were performed in Matlab to infer statistical significance for system parameters on jet speed and shape.

3 Results and discussion

3.1 Spark-induced cavitation

To study the dynamics of spark-induced cavitation bubbles, our setup depicted in Fig. 1 was modified to allow a spark to be generated inside a transparent plexiglass tank filled with water. The electrical breakdown at the spark point immediately vaporizes the water in the vicinity of the spark point, leading to the formation of a cavitation bubble. This bubble expands to a maximum size and then collapses. Figure 2 shows snapshots that depict the dynamics of cavitation bubbles for capacitance $C = 1000$ μF and increasing discharge voltages of (A) 30 V, (B) 45 V, and (C) 60 V.

After the spark, a nearly spherical cavitation bubble expands and reaches a maximum size over time, as can be seen from the snapshots. The typical time from the onset of the spark to reaching maximum bubble size is on the order of hundreds of microseconds ($\tau \approx 200$, 300, 400 ms, respectively, for $C = 1000\,\mu$F and $V_d = 30$, 45, and 60V), as seen in the bubble radius evolution in Fig. 3. During expansion, the cavitation bubble can be seen to contain plasma generated from the spark, evident from the saturated pixels, indicating intense localized heating. After attaining a maximum size during expansion, this bubble collapses violently, creating a cloud of smaller bubbles, fumes and gas (see $t =$ 50 and 100 ms in Fig. 2). The source of fumes and gases was the burning of brass electrodes during a spark. As expected, we observed that the size of the cavitation bubble increased with an increasing discharge voltage and the capacitance of the capacitor, as shown in Fig. 4. Following the analyses in Avila et al. (2015); Palanker et al. (1997), we estimate the potential energy stored in the bubble as $E_{\text{bub}} = PV_{\text{max}}$, where P is taken to be the atmospheric pressure and V_{max} is the maximum volume of the bubble. From image analysis of the bubble at maximum size, we estimate $V_{\text{max}} \approx 18.6$, 151, and 486 mm^3 for discharge voltages of $V_d = 30$, 45, and 60 V, respectively. These lead to bubble energies of $E_{\text{bub}} \approx 1.8$, 15.3, and 49.2 mJ, respectively. The overall efficiency of energy conversion can then be garnered from $\eta = E_{\text{bub}}/E_d$, where E_d represents the overall electrical energy available for spark discharge, calculated from capacitance, C, and charging voltage, V_d, as $E_d = \frac{1}{2}CV_d^2$. For the data in Fig. 4 with $C = 1000$ μF, we find the efficiencies to be in the range 0.4–3.8 %, in reasonable agreement with previous findings (Buogo et al. 2009). Furthermore, in accordance with estimates in Buogo et al. (2009), it is expected that the majority of the balance of the discharge energy is dissipated via Joule heating ($\sim 80\%$) and optical radiation ($\sim 11 - 17\%$).

3.2 Spark-induced jetting

To promote jetting in a controlled manner, the spark setup was placed in a capillary tube containing liquid, with one end open to air and the other end connected to a syringe filled with liquid (Fig. 1E). The distance between the meniscus and the spark point was initially kept constant at $L_m =$ 3 mm, which implies a maximum volume of 24 μL between the electrodes and the open end, although the concave meniscus reduces this slightly. The liquid level (meniscus location) inside the tube was controlled through a syringe pump.

Figure 5 shows snapshots of spark-induced jetting in DI water for discharge voltages of 30–60 V from a 4700 μF capacitor. Inspecting figure (A) for $V_d = 30$V, we observe that electrical breakdown at the junction of two electrodes first creates a shock-wave that impacts and rapidly deforms the meniscus. Due to the concavity, the impulse pressure from the shock wave first hits the highest point of the meniscus (in the center of the tube); therefore, the tip of the jet first emerges from the center. In most cases, optical saturation due to the plasma generation hinders the visibility of the cavitation bubble ($t \approx 0.25 - 0.5$ ms); however, we can

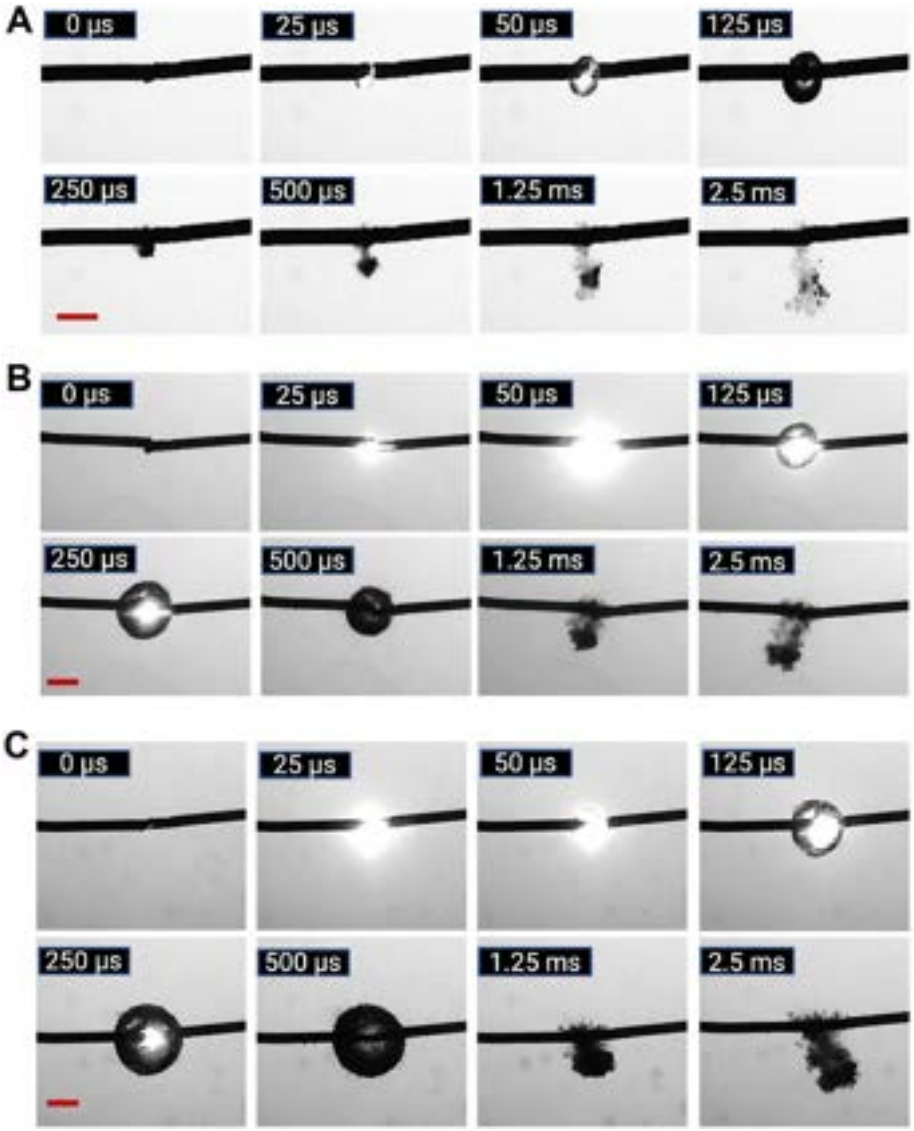

Fig. 2 Snapshots showing the formation and subsequent collapse of a cavitation bubble for a 1000 μF capacitor discharged inside DI water for voltages of **A** 30 V, **B** 45 V, and **C** 60V. *Scale bars represent 2 mm*

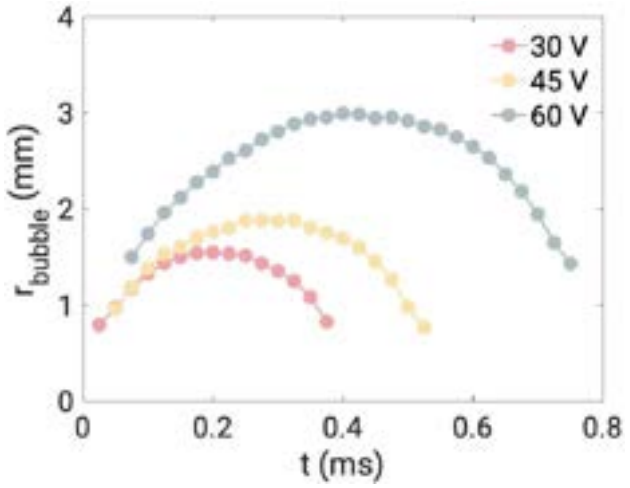

Fig. 3 Bubble radius with time for different voltages with a 1000 μF capacitor

infer that as the cavitation bubble expands, more liquid is forced through the opening of the tube which, in addition to momentum of the tip, serves to temporarily sustain the jet flow. As the bubble collapses and oscillates, the liquid jet becomes weaker and breaks up at multiple locations and fragments into multiple droplets, as shown in the last frame ($t = 6.75$ ms) of Fig. 5(A). Dark regions observed at $t \geq 1.25$ ms near the electrodes are a combination of micro-bubbles from the collapse, and gases formed from burning of brass wires.

Figure 5(B) shows spark-induced jetting snapshots for a discharge voltage of 45 V. In this case, the liquid jet was significantly faster than for $V_d = 30$ V, as the jet traveled farther in a short time compared. The optical saturation due to the spark lasts for a longer time ($t \sim 2$ ms) due to more extensive plasma generation. In addition, higher discharge energy leads to a larger bubble (as per Fig. 4), therefore leading to

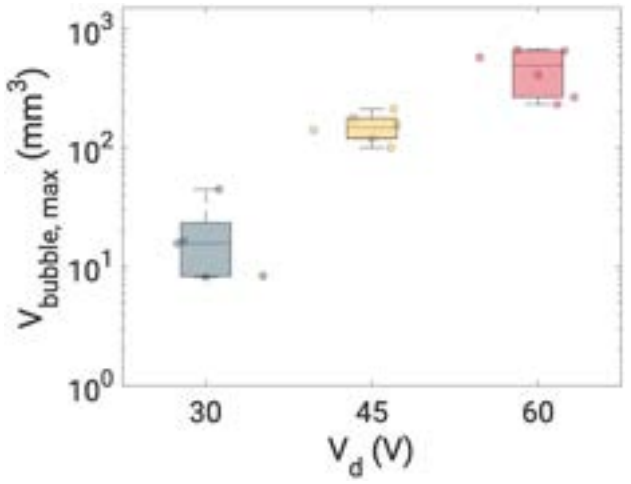

Fig. 4 Maximum bubble volumes ($V_{bubble,max}$) estimated from image analysis (e.g., Fig. 3) assuming spherical equivalent diameters for DI water for a capacitance of $C = 1000\ \mu$F

a larger volume of liquid being expelled in comparison with lower voltages. This can be readily seen by inspection of the jet at $t = 1.5$ ms, which is markedly thicker and longer than the jet in Fig. 5A. At this higher discharge voltage, we also note a thicker liquid column approximately equal in diameter to the capillary inner diameter (see arrows in the second frame at $t = 0.5$ ms); This again is an indication of a larger bubble, which has expands and displaces a larger volume of water from the space between the spark point and the open end. This liquid jet then thins with further propagation as the bubble starts to collapse and the kinetic energy of the liquid diminishes and leads to a bulbous shape (third and fourth frames at $t = 1$ and 1.5 ms) marking the separation between the focused jet and the liquid column. At later times ($t > 1.5$ ms), the jet continues to travel downward and thin out, while concurrent bubble oscillations manifest in secondary expulsion of liquid in the form of liquid drops.

At the maximum discharge voltage, $V_d = 60$ V, determined by the voltage rating of the capacitors (63 V) used, we observe the process to be even more violent, as seen in the snapshots presented in Fig. 5(C). Following the observations at $V_d = 45$ V, the more extensive bubble expansion leads to an even more pronounced kink, indicated by the arrows in the third frame at $t = 0.4$ ms and the dashed outline in the fourth frame at $t = 0.75$ ms. Given the higher discharge energy, and data in Fig. 4, one would expect a larger volume to be expelled. However, the bubble collapse appears to be more violent and the negative pressure effectively severs the jet, as indicated in the fifth frame at $t = 1.75$ ms. Therefore, the remaining liquid expelled is not a coherent jet, but fragmented into droplets. This is clearly an undesirable feature from the perspective of applications such as precise jet deposition or drug delivery. Finally, we also observed that

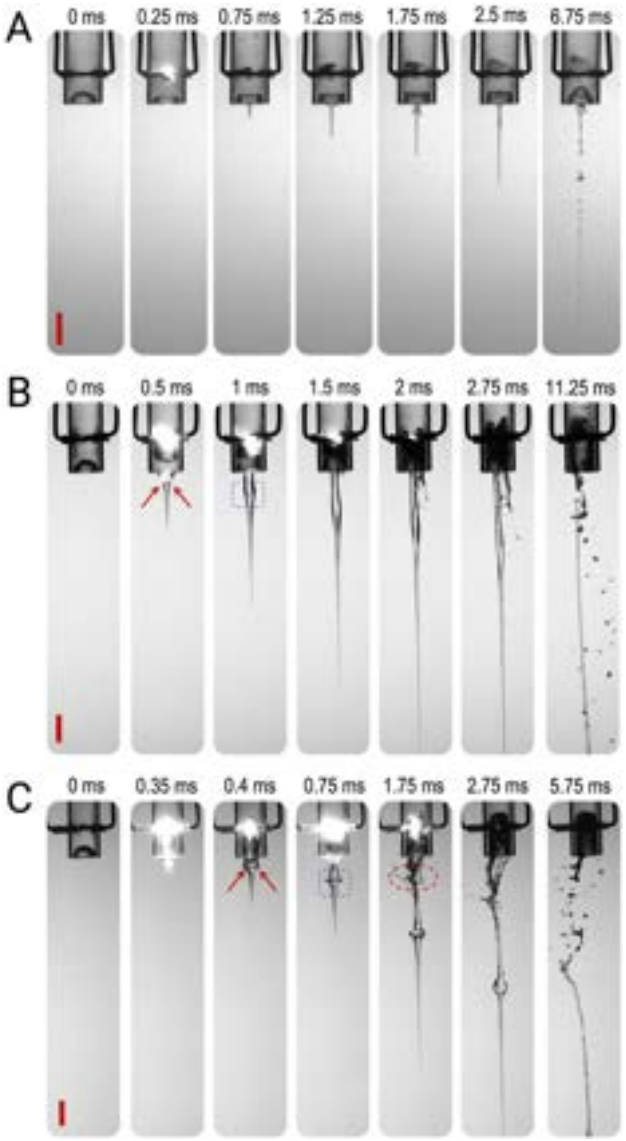

Fig. 5 Snapshots showing spark-induced jets for a 4700 μF capacitor discharged inside DI water at **A** 30 V, **B** 45 V, and **C** 60 V. *Scale bars represent 5 mm*

the liquid remaining in the tubes after sparking at higher voltages contained microscopic brass particles and gases generated from burning of brass wires. This effect was most pronounced for $C = 4700$ muF due to higher overall energy, and the electrodes exhibited disintegration, whereas this was not observed for $C = 1000$ muF.

3.3 Effect of discharge voltage

To capture the effect of discharge energy on jet speed, we varied both the capacitance ($C = 1000$ and 4700 μF) and the charging voltage ($V_d = 30 - 60$ V). Figure 6 summarizes the effect of discharge voltage and capacitance on

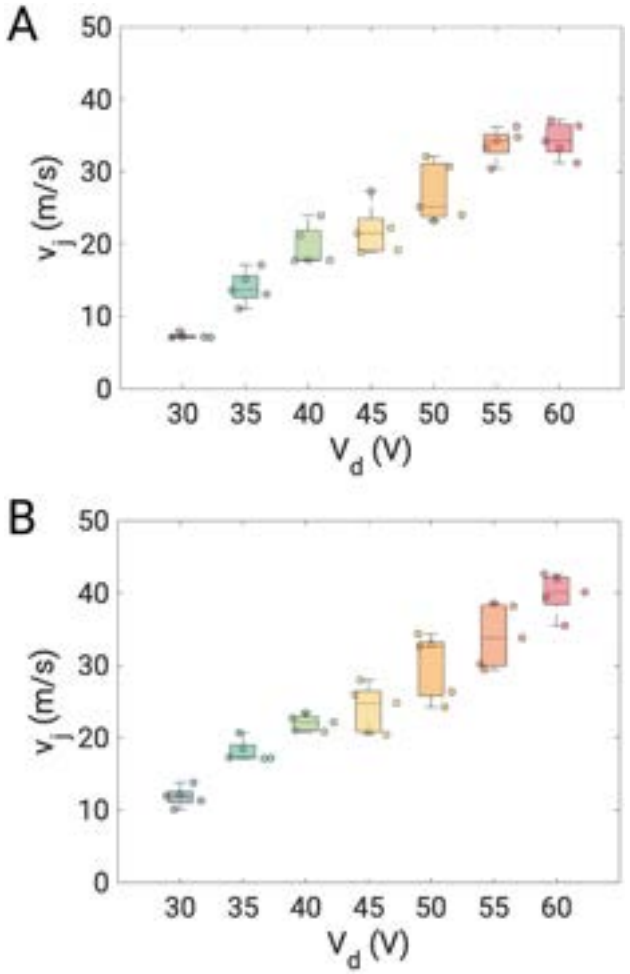

Fig. 6 Effect of discharge voltage on the jet tip speed for capacitance of **A** $C = 1000$ muF and **B** $C = 4700$ muF. In all cases, $L_m = 3$ mm, $D_i = 3.2$ mm. A minimum of 5 repeat trials were performed for each voltage ($n \geq 5$)

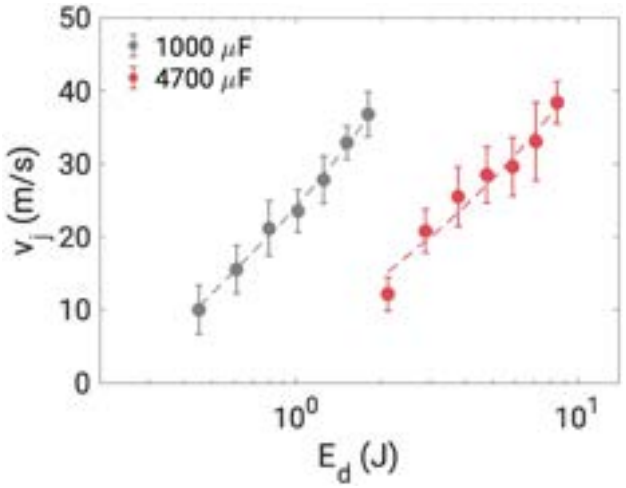

Fig. 7 Effect of discharge energy on the jet tip speed for both capacitors ($C = 1000$ µF and $C = 4700$ µF) with constant $L_m = 3$ mm. The dashed lines represent power law fits of the form $v_j = 29.53(E_d - 0.3125)^{0.53}$ ($R^2 = 0.995$) for 1000 μF and $v_j = 14(E_d - 0.94)^{0.49}$ ($R^2 = 0.952$) for 4700 μF

the jet tip speed, measured by frame-to-frame analysis from images such as those in Fig. 5. We observe that the jet speed increases monotonically in a near-linear fashion from $v_j \sim 7 - 37$ m/s as $V_d : 30 \rightarrow 60$ V for $C = 1000$ μF (see Fig. 6A). Similarly, for the case of $C = 4700$ μF, the jet speed increases from $v_j \sim 10 - 42$ m/s for the same voltage range (Fig. 6B). Note that the experimental voltage range was limited to 30–60 V due to the capacitor rating of 63 V and that for $V_d < 30$ V, no liquid jet was observed. The collective effect of V_d and C in terms of discharge energy ($E_d = 0.5CV_d^2$) on the jet speed (v_j) is summarized in Fig. 7.

We can rationalize these observations by considering that the discharge energy is converted to kinetic energy, which varies as v_j^2. As such. we expect the jet speed to vary with the square root of the discharge energy, according to the heuristic equation $v_j \propto (E_d - E_{\min})^{1/2}$, where $E_{\min}$ is the threshold energy required to form a jet. The best power law fits of this type provide an excellent description of the data, with power-law exponents of 0.53 and 0.49, and correlation coefficients of $R^2 = 0.99$ and 0.95, respectively.

The kinetic energy of the jet ($E_k = \frac{1}{2}Mv_j^2$) could be estimated based on the mass of water ejected which, with $D_i = 3.2$ mm and $C = 1000$ μF, ranged from $M \approx 3 - 50$ depending on the exact configuration. Combined with the range of jet velocities, $v_j = 7 - 40$ m/s, this yields kinetic energies in the range $E_k \approx 0.16 - 40$ mJ. It is acknowledged that this is certain to be an overestimate since this calculation assumes a constant ejection speed for the whole jet mass, which is not the case. Notwithstanding this caveat, the conversion efficiency from the overall energy available for spark discharge, E_d, to the jet kinetic energy, E_k is in the range of 0.03–2%.

Taking into account the jet diameter of ~ 300 μm (*near the jet tip*) and the initial exit speeds from Fig. 7, Reynolds numbers for the water jets were in the range of $Re \approx 3,000 - 12,600$. Based on previous literature (e.g., [26], citing a transition to turbulence around $Re \sim 10^3$, this would indicate that the liquid flow is turbulent; however, it should be noted that the Reynolds number defined therein was based upon the nozzle orifice diameter, which is not strictly applicable to our case since the flow focusing creates a jet tip which is significantly thinner than the inner diameter of the capillary. Furthermore, the slender appearance of the jet tip immediately after exiting does not exhibit the hallmarks of turbulent jet flow emanating from a nozzle. For lower voltages ($V_d \leq 30$ V), the jet break-up (e.g., Figs. 5A,

10A, 11A) is also smooth, characteristic of laminar flow. However, at higher voltages ($V_d \geq 40$ V), the rapid collapse of the cavitation bubble inside the tube creates a more violent appearance during jet break-up (e.g., Figs. 5C, 10C, 11C), where the flow may be turbulent.

Lastly, it is noteworthy that the jet speed generated by a 1000 μF capacitor are comparable to those obtained with a 4700 μF capacitor over the same voltage range. Therefore, the higher discharge energy for 4700 μF does not significantly affect the jet speed compared to the 1000 μF capacitor. One possible explanation is that higher discharge energies result in a higher conversion to Ohmic heating and optical radiation (as evident in the intense photoemissions at higher voltages) and therefore have a lower fraction available for bubble potential energy. Additionally, the proximity of the sparking point to the meniscus and the geometric constraints of the capillary tube restrict the growth of bubbles, limiting the overall conversion of electrical energy to kinetic energy. Furthermore, for a lower capacitance of 1000 μF, the spark caused less damage to the brass electrodes, suggesting that this configuration is preferable for spark-induced liquid jets from confined geometries.

3.4 Effect of spark location

The available volume for ejection can be controlled by changing the location of spark point with respect to the liquid meniscus (i.e., L_m, as indicated in Fig. 8A) inside the capillary tube. To isolate this effect, we varied L_m for a constant discharge voltage of $V_d = 45$ V and capacitance $C = 1000$ μF ($E_d = 1.01$ J). Three different locations of the spark point were used that correspond to $L = 3$ mm, 7 mm, and 11 mm.

Figure 8(B) shows the results for the jet speed, v_j, plotted against L_m for the DI water as the fluid. With an increase in L_m, the discharge energy is dissipated to a larger volume of liquid and a larger surface area of the cylindrical tube. Therefore, the kinetic energy imparted per unit volume of liquid before reaching the meniscus is lower for larger L_m, resulting in a lower jet speed. For a discharge energy of ~ 1.01 J, the estimated kinetic energy was in the range of ~ 0.025−0.11 mJ for L_m decreasing from 11 to 7 mm. From a statistical standpoint, the effect of the location of the spark point on the jet speed was highly significant ($p < 0.01$) for L_m changing from 3→7 mm and 3→11 mm, but not significant ($p > 0.05$) for an increase in L_m from 7-11 mm. Another relevant observation with regards to practical implementation is that higher values of L_m (7 and 11 mm) leave bubbles inside the liquid column after jet ejection, whereas a lower value of L_m (3 mm) not only provides a liquid jet with higher jet speed but also leaves the liquid inside the tube relatively free of cavitation bubbles. This indicates that a shorter distance between the sparking point and the meniscus is preferential for potential repetitive jetting regimes (Krizek et al. 2020).

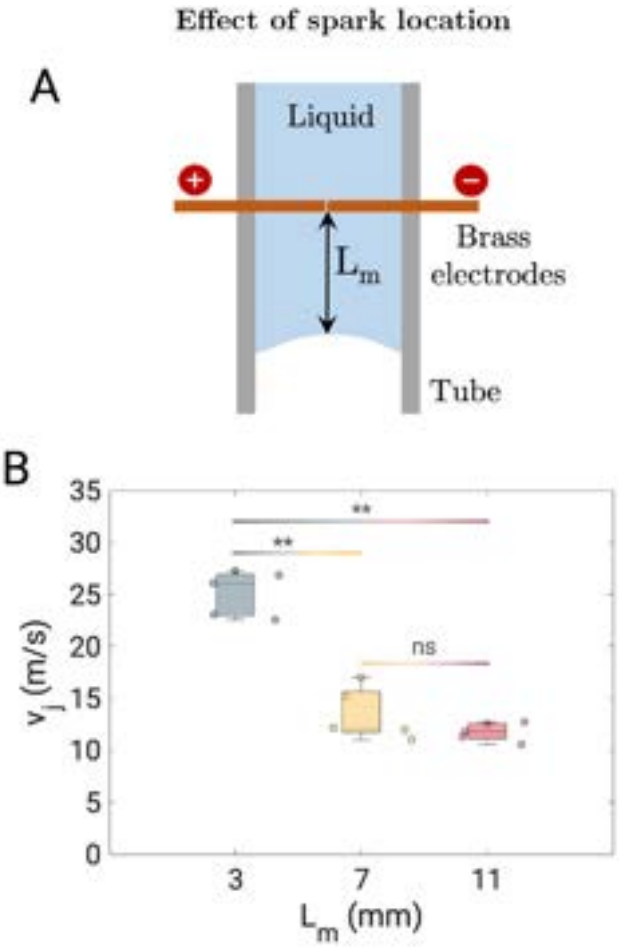

Fig. 8 Effect of L_m on the jet speed. **A** Schematics showing the definition of L_m and **B** jet speed (v_j) versus L_m for a voltage of 45 V discharged from a 1000 μF capacitor. ($n = 5$)

3.5 Jet breakup length

Liquid jet break up is a well-known phenomenon, primarily governed by a competition between inertia and surface tension, and associated with the Rayleigh-Plateau instability. A descriptive example is presented in Fig. 9(A) showing the process of liquid jet break up and jet breakup length for a water jet generated for 4700 μF capacitor. In this realization, the liquid jet thins in front and ruptures at a critical value for the length of the jet, known as the jet break-up length ($L_{\text{jet}-\text{breakup}}$) (see Fig. 9A), and results in the formation of a single drop ($t = 35$ ms) followed by the formation of multiple satellite droplets ($t = 135$ ms).

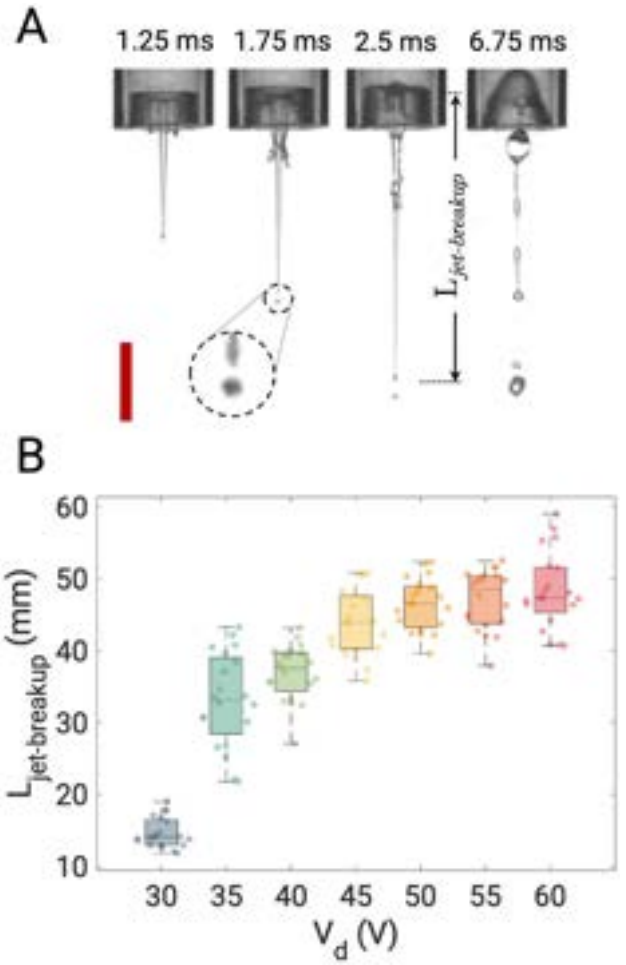

Fig. 9 Jet break-up length for water jets generated for different discharge voltages from a 4700 μF capacitor. **A** Snapshots showing jet break-up for $V_d = 30$ V with $L_{jet-breakup} \approx 18$ mm. Scale bar represents 5 mm. **B** Jet break-up length plotted as a function of discharge voltage

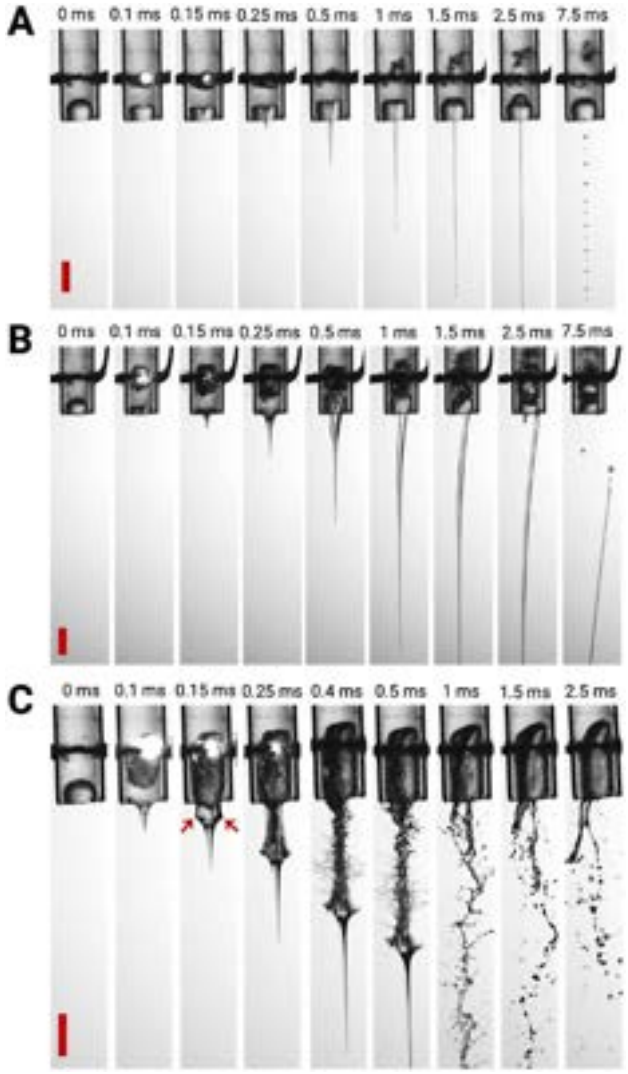

Fig. 10 Snapshots showing spark-induced jets of 50% glycerol for a 1000 μF capacitor discharged at **A** 30V, **B** 45V, and **C** 60V with $L_m \approx 3$ mm. *Scale bars represent 5 mm*

A summary of our measurements across the range of discharge voltages is presented in Fig. 9(B). We observed that the jet break up length increased rapidly from $L_{jet-breakup} \approx 13$ mm to ≈ 45 mm as V_d increased from 30 V to 45 V, but further increase in V_d up to 60 V did not result in any appreciable increase in break up length, saturating at $L^*_{\text{jet}-\text{breakup}} \approx 50$ mm. Across the entire data range, the effect of voltage on break up length was found to be statistically significant ($p \ll 0.01$).

Again, from a practical perspective, a coherent (streamline and intact) jet with constant speed is desirable for purposes of fluid delivery, for example in needle-free drug delivery. Therefore, an early jet breakup is an undesirable feature.

3.6 Viscous jets

In this section, we present a qualitative overview of viscous jetting via spark-induced cavitation followed by a quantitative analysis of the jet speed for varying viscosity and discharge voltage. To understand the effect of viscosity, we chose to perform repeat experiments in two different aqueous glycerol mixtures - 50%$_{w/w}$ glycerol and 80%$_{w/w}$ glycerol. These weights were selected since they increase the viscosity by approximately an order of magnitude each compared to water, i.e., $\mu_{50\,G} \sim \mathcal{O}(10^1)$ mPa s and $\mu_{80\,G} \sim \mathcal{O}(10^2)$ mPa s, respectively.

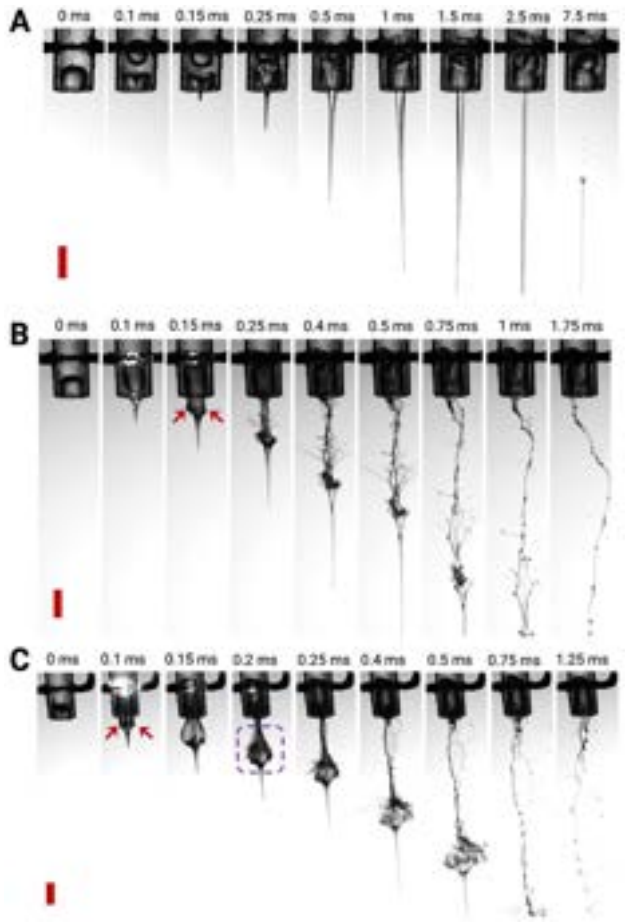

Fig. 11 Snapshots showing spark-induced jets of 80% glycerol for a 1000 μF capacitor discharged at **A** 30V, **B** 45V, and **C** 60V. $L_m \approx 3$ mm. Scale bars represent 5 mm

To begin, we demonstrate the effect of viscosity for a 1000 μF capacitor at three different discharge voltages (30, 45, and 60 V), as shown in Fig. 10. In general, the process remains qualitatively similar to water in that the initial pressure impulse creates a focused jet tip, then as the bubble expands, more volume is expelled from the tube. However, there are a few notable differences. First, the photo-emissions are significantly reduced (the bright spots from the spark-induced plasma are smaller and shorter-lived) indicating that a smaller fraction of the discharge energy is dissipated by optical and thermal means. Second, the jets are markedly more slender and coherent than for water (compare with Fig. 5), and the jet tip is faster, evident from the distance traveled in the first ~ 1 ms compared to the water jets.

In Fig. 10(A), the jet break-up time and length were delayed compared to water, but occurred before $t \sim 7.5$ ms. This effect is also seen in Fig. 10(B) for higher discharge voltage, while the curved jet for $t \geq 1.5$ ms in that specific realization appears to be a manifestation of asymmetric bubble collapse and oscillation inside the tube. The jet for $V_d = 45$ V is considerably thicker, for example at $t \approx 1$ ms, the jet diameter in Fig. 10(A) (measured near the tube opening) is $d_{\text{jet}} \approx 0.7$ mm, while in Fig. 10(B) it is $d_{\text{jet}} \approx 1.6$ mm. This increased thickness corresponds to an increased bubble volume, as per our prior observations.

Finally, for the highest discharge voltage of 60 V (Fig. 10C), the spark-generated cavitation bubble was even larger in size and pushes the liquid as a column (compare images at $t = 0.1 - 0.15$ ms in all cases). The focused and tapered part of the liquid jet was again much faster than for lower voltages and occurred in front of a pronounced kink marked by the red arrows at $t = 0.15$ ms. The subsequent thick jet is subject to instability from the violent collapse and oscillation of the bubble ($t = 0.25 - 0.5$ ms), then fragments into small droplets, as the whole jet elongates ($t = 1 - 2.5$ ms).

Corresponding image sequences of the higher-viscosity jets for 80% glycerol are presented in Fig 11. Interestingly, for the lowest discharge of $V_d = 30$ V, the cavitation bubble was *larger* than that observed in the case of 50% glycerol. The resulting jet was also thicker and faster than that obtained for less viscous fluids. Consequently, the time before jet breakup was also longer.

For higher voltage of 45 V, only a short focused jet is expelled before a thick liquid column is ejected. The red arrows at $t = 0.15$ ms mark the boundary between the thin and thick sections. In a similar fashion to Fig. 10(C), the thick part of the jet is subject to fragmentation. The fact that the thick jet emerges sooner (at lower voltage compared to 50% glycerol) indicates that bubble growth is more rapid and more extensive in this more viscous fluid. Noting also that the photo-emissions are less intense again points to less energy dissipation via heat.

This effect becomes even more pronounced at the highest voltage of 60 V, shown in Fig. 10(C), with an even shorter jet tip ($t = 0.1$ ms). In this instance, however, we note that the thick part of the jet takes an annular or 'balloon' structure, whereby the vapor bubble has become incorporating into the jet. This collapses as the jet travels downward ($t = 0.25 - 0.5$ ms) concurrent with fragmentation of the liquid behind it.

Although the viscous jets for 45 V and 60 V have higher jet tip speed, the shape of the jet and the fragmentation make them undesirable from the perspective of applications in inkjet printing, drug delivery, surface coatings, etc., and hence should be avoided.

The quantitative effect of viscosity on the jet tip speed is presented in Fig. 12(A). For $V_d = 30$ V, the jet speed increased from ~12 m/s for water to ~20 m/s for 50% glycerol. However, for an approximately ten-fold increase in fluid viscosity from 50% glycerol to 80% glycerol, jet speed increases by only ~1 m/s. For a voltage discharge of 45 V, the jet speed increased from ~24 m/s to 42 m/s,

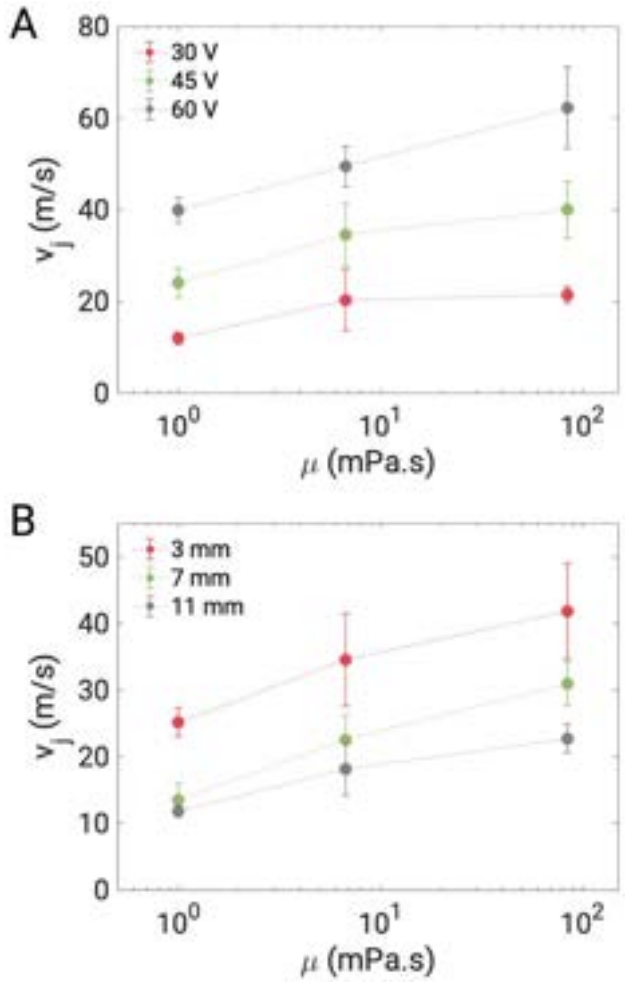

Fig. 12 Effect of viscosity on the jet speed for different **A** discharge voltages (with $L_m \approx 3$ mm) and **B** distance of spark point from the meniscus (with $V_d = 45$ V). Data points are the average of 5 repeat trials

for an increase in viscosity from ~1 to ~84 mPa.s. For the liquid jets generated for the higher voltage discharge of 60 V, the increase in the jet speed was linear from ~40 m/s for water to ~62 m/s for glycerol. The effect of viscosity was statistically significant on the jet speed ($p < 0.05$) for different voltages used here.

Furthermore, the effect of viscosity was also studied for constant voltage and different locations of the spark point with respect to the meniscus (Fig. 12B). The jet speed increased with viscosity in a near-linear fashion for different values of L_m. As discussed earlier, increasing L_m resulted in decreasing jet speed and same was observed for different fluids with varying viscosity. Interestingly, for viscous fluids, the effect of the location of the spark point was more significant on the jet speed compared to that of water. Overall, the effect of viscosity was also significant on the jet speed ($p < 0.05$) for varying L_m.

Overall, regardless of the voltage or location of the spark relative to the meniscus, the effect of viscosity was the *increase* jet speed. This seemingly counterintuitive observation could be explained by the fact that the electric breakdown threshold for aqueous glycerol solutions is lower than that of pure water, leading to more extensive bubble growth. However, for higher discharge voltages, the jets for 50% and 80% glycerol were subject to break-up and fragmentation arising from the violent bubble collapse and oscillation. For 50% glycerol at $V_d \leq 45$ and 80% glycerol at $V_d = 30$V, fast and slender jets were produced with delayed break-up time. These jet characteristics may be useful for applications.

As a final illustrative example, we present Fig. 13, showing the impact of a spark-induced jet of 50% glycerol onto a glass substrate, which is placed approximately 12 mm below the capillary. Here, we can see that the (vertical) jet momentum is dissipated horizontally as it impacts the substrate, creating a well-known hydraulic jump (see panel (iii)). This impact-spreading process has recently been documented as a means of depositing viscous paints (Kamamoto et al. 2021) and is therefore worthy of a more detailed investigation.

4 Conclusions and outlook

In conclusion, we demonstrate the feasibility of a low-voltage discharge technique for generating spark-induced liquid jets. From the parameters studied, the discharge voltage, capacitance, location of the spark point, and viscosity of the liquid significantly affected the jet dynamics and the jet speed. In general, the jet ejected has a focused, fast tip, which is the result of the pressure impulse impacting the concave meniscus. Then, as the breakdown of the liquid creates plasma and Ohmic heating, a vapor bubble grows, which expels more liquid due to volume displacement. This led to a two-stage jet structure with a thin, fast tip and a thicker, slower column behind it. Some crude calculations of energy conversion indicated that only a fraction (< 2%) of the discharge energy is converted to jet kinetic energy, in accordance with prior publications in this area. Nonetheless, jet speeds up to 60 m/s were produced, with the fastest jets occurring for the higher viscosities. From the perspective of applications, a coherent, streamline jet is preferable to the two-tier fragmented jets (observed for higher discharge energies, and lower viscosities). As such, our limited study indicates an optimal range of parameters as follows: $C = 1000\ \mu$F, $V_d \leq 45$ V, $\mu \sim \mathcal{O}(10)$ mPa s, $L_m \leq 5$ mm. We also acknowledge various system limitations of the spark-induced jetting phenomenon described herein as follows:

1. The presence of bubbles from undissolved or non-condensable gas after a single discharge may affect the repeatability and consistency of liquid jets, since they

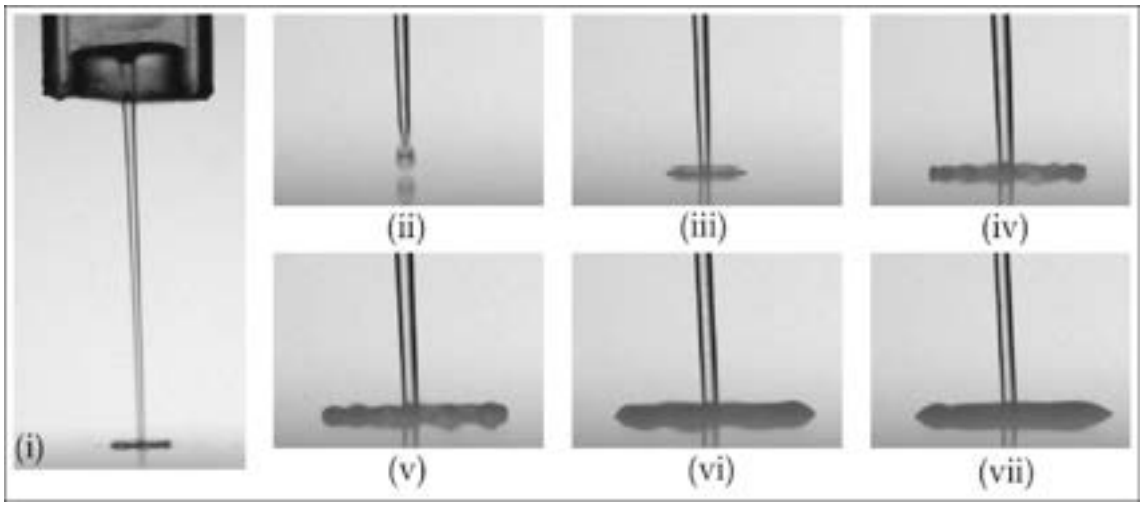

Fig. 13 Impact of a spark-induced jet onto a glass substrate placed approximately 12 mm below the capillary tube (D_o = 6.3 mm, V_d = 35 V, $L_m \approx$ 3 mm). The overview figure on the left (i.e., panel (i)) shows the jet at t = 3 ms, while the zoomed images to the right show the impact-spreading phenomena at (ii) $t = -0.5$ ms, (iii) t = 0.5 ms, (iv) t = 4.7 ms, (v) t = 9.5 ms, (vi) t = 19.5 ms, (vii) t = 29.5 ms

will influence the energy absorbed from subsequent discharges. However, since we could not directly measure their presence or extent, this factor could not be quantified.

2. Positioning of the wires and the exact shape of the contact area is very difficult to replicate exactly and may also contribute to variation in jet speed for a given configuration.
3. The presence of remnants of electrode material due to disintegration after the spark in the jet is clearly undesirable for applications such as inkjet printing, drug delivery and surface coating.
4. Occasionally, wires are touched multiple times due to oscillations in the cavitation bubble, leading to multiple sparks and inconsistent jets.

The highest jet speed observed herein was approximately 60 m/s, which therefore makes the current system nonviable for intradermal drug delivery; typically, the initial jet speed required to puncture skin for purposes of needle-free injection is of the order of 150–200 m/s. After the initial puncture, the "follow-up" jet speed (for the remainder of the injection) will determine how deep the injection goes—i.e., for deeper intramuscular injections, it is desirable to maintain a higher jet speed, whereas for shallow intradermal injections, it is desirable to reduce the jet speed to around 60–100 m/s (McKeage et al. 2018). To pursue such an application using spark-induced jets, it is proposed to extend this study by incorporating effects such as tapered geometry and additives to the liquid. Furthermore, our illustrative example of the jet impact-spreading process revealed some intriguing features that will be expounded upon in a subsequent publication.

Acknowledgements We would like to acknowledge Alexandria Banks, Hieu Nguyen and Lawrence Lewis, undergraduates from Electrical Engineering at Texas Tech, for their help with the initial design and experiments.

Author Contributions JM conceptualized the research; PR conducted and analyzed experiments and prepared all figures. Both authors wrote and reviewed the manuscript.

Funding This work was financially supported by the National Science Foundation through award number CBET-1749382.

Data availability Data will be made available upon request to the corresponding author.

Declarations

Conflict of interest The authors declare no competing interests.

Ethical approval Not applicable.

References

Albright PS (1937) Experimental tests of recent theories descriptive of the salting-out effect. J Am Chem Soc 59:2098–2104

Avila SRG, Song C, Ohl C-D (2015) Fast transient microjets induced by hemispherical cavitation bubbles. J Fluid Mech 767:31–51

Blake JR, Gibson DC (1987) Cavitation bubbles near boundaries. Ann Rev Fluid Mech 19:99–123

Brennen CE (2014) Cavitation and bubble dynamics. Cambridge University Press, Cambridge

Brujan E-A, Nahen K, Schmidt P, Vogel A (2001) Dynamics of laser-induced cavitation bubbles near elastic boundaries: influence of the elastic modulus. J Fluid Mech 433:283–314

Buogo S, Plocek J, Vokurka K (2009) Efficiency of energy conversion in underwater spark discharge and associated bubble oscillations: eperimental results. Acta Acustica 95:46–59

Burrill LC (1951) Sir Charles Parsons and cavitation. Inst Marine Eng Trans. Vol. LXIII, No. 8

Chaves H, Knapp M, Kubitzek A, Obermeier F, Schneider T (1995) Experimental study of cavitation in the nozzle hole of diesel injectors using transparent nozzles. SAE Trans 104(3):645–657

Davies RM, Taylor GI (1943) The motion and shape of the hollow produced by an explosion in a liquid. Sci Papers of GI Taylor 3:337–353

Dijkink R, Ohl C-D (2008) Laser-induced cavitation based micropump. Lab Chip 8(10):1676–1681

Fletcher DA, Palanker DV, Huie P, Miller J, Marmor MF, Blumenkranz MS (2002) Intravascular drug delivery with a pulsed liquid microjet. Arch Ophthalmol 120(9):1206–1208

Gautner JW, Livingwood JNB, Hrycak P (1970) Survey of literature on flow characteristics of a single turbulent jet impinging on a flat plate. NASA Tech Rep, TN D-5652

Goh BHT, Oh YDA, Klaseboer E, Ohl S-W, Khoo BC (2013) A low-voltage spark-discharge method for generation of consistent oscillating bubbles. Rev Sci Instrum 84(1):014705

Gordillo JM, Onuki H, Tagawa Y (2020) Impulsive generation of jets by flow focusing. J Fluid Mech 894:A3

Green DW, Southard MZ (2019) Perry's chemical engineers' handbook. McGraw-Hill Education, Columbus

Kamamoto K, Onuki H, Tagawa Y (2021) Drop on demand painting of highly viscous fluids. Flow 1:E6

Karri B, Ohl S-W, Klaseboer E, Ohl C-D, Khoo BC (2012) Jets and sprays arising from a spark-induced oscillating bubble near a plate with a hole. Phys Rev E 86(3):036309

Kling CL, Hammitt FG (1970) A photographic study of spark-induced cavitation bubble collapse. Tech Rep No. UMICH 03371-4-T

Krizek J, Delrot P, Moser C (2020) Repetitive regime of highly focused liquid microjets for needle-free injection. Sci Rep 10:5067

Lew KSF, Klaseboer E, Khoo BC (2007) A collapsing bubble-induced micropump: an experimental study. Sens Actuators A 133(1):161–172

McKeage JW, Ruddy BP, Nielsen PMF, Taberner AJ (2018) The effect of jet speed on large volume jet injection. J Control Release 280:51–57

Osman OO, Abouel-Kasem A, Ahmed SM (2022) Shock waves as dominant mechanism for cavitation damage. J Tribol 144(6):062301

Palanker D, Turovets I, Lewis A (1997) Electrical alternative to pulsed fiber-delivered lasers in microsurgery. J Appl Phys 81(11):7673–7680

Podbevsek D, Lokar Z, Podobnikar J, Petkovsek R, Dular M (2021) Experimental evaluation of methodologies for single transient cavitation bubble generation in liquids. Exp Fluids 62:1–28

Rohilla P, Marston J (2020) Feasibility of laser induced jets in needle free jet injections. Int J Pharm 589:119714

Shima A, Takayama K, Tomita Y, Ohsawa N (1983) Mechanism of impact pressure generation from spark-generated bubble collapse near a wall. AIAA J 21(1):55–59

Tagawa Y, Oudalov N, El Ghalbzouri A, Sun C, Lohse D (2013) Needle-free injection into skin and soft matter with highly focused microjets. Lab Chip 13(7):1357–1363

Tagawa Y, Oudalov N, Visser CW, Peters IR, van der Meer D, Sun C, Prosperetti A, Lohse D (2012) Highly focused supersonic microjets. Phys Rev X 2(3):031002

Vandiver JK, Wales CA (1977) High-speed photography of transient cavitation on marine propellers. In: 12th Intl congress on high speed photography, SPIE, volume 97, pages 172–176